Status on Plasma Diagnostic Measurements on a RIT-10 Ion Thruster

IEPC-2007-173

Presented at the 30th International Electric Propulsion Conference, Florence, Italy
September 17-20, 2007

Michael W. Winter *, Christoph Eichhorn †, Monika Auweter-Kurtz‡, and Thomas Pfrommer §
Universität Stuttgart, Institut für Raumfahrtsysteme (IRS), Pfaffenwaldring 31, 70550 Stuttgart, Germany

First plasma diagnostic investigations of the plume of a RIT-10 ion thruster with xenon as propellant are presented. Emission spectroscopic measurements were taken at axial distances between 60 mm and 150 mm to the acceleration grid and at radial positions between the thruster axis and 45 mm distance to it, respectively. Excitation temperatures and pParticle densities of neutral and singly ionized Xenon are determined based on the assumption of Boltzmann distributions for the electronically excited states. The evaluation will be extended to a more detailed modelling (e.g. Corona model) as soon as supporting data from Fabry-Perot interferometry and Lagmuir probes are available. The Fabry-Perot set up is already completed but no data has been taken yet. The application of 2 photon LIF to the plume of the ion thruster has been preliminarily rejected for the time being since experiments conducted with a cold gas cell have been shown that the required pressures are too low to yield reliable results with the available set up. However, recent data show that eventually the sensitivity of the set up might be increased by using different excitation schemes. Therefore, the experiments on the cold gas cell are continued to further investigate this possibility.

I. Introduction

At the Institute of Space Systems (IRS) of the University of Stuttgart, non-intrusive diagnostic methods have been under investigation for plasma thrusters as well as for reentry plasmas since more than a decade [1]. Recently, a test stand was prepared for ion thruster testing [2] to be used with an RIT-thruster from EADS-ST [3] for plasma diagnostic investigation of the plume and the plasma properties close to the grids. Ion thrusters have attracted the attention of satellite manufacturers for a long time because of their high specific impulse and efficiency. For physical reasons, one of the most promising propellants is xenon. The investigation of local characteristics of the xenon plasma by means of non-intrusive methods is a very important task for understanding the processes in these thrusters. For this purpose, spectroscopic techniques for the ion thruster plume investigations are currently under development at IRS [2]. Two-photon laser-induced-fluorescence for density measurements on neutral xenon has already been performed in a cold gas cell [4]. Emission spectroscopy, electrostatic probes and Fabry-Perot interferometry were used for preliminary measurements in a xenon plasma produced by a microwave generator [5], [6]. The emission spectroscopic measurements showed a strong non-equilibrium situation in the plasma. Although only weak ion emission could be detected, the electrostatic probe measurements showed electron densities in the order of 10^{18} m^{-3} and distributions of the electron temperature between 20000 K and 60000 K. Because the

* Scientist, Institute of Space Systems (IRS), winter@irs.uni-stuttgart.de .
† PhD student, IRS, eichhorn@irs.uni-stuttgart.de .
‡ President of the Universität Hamburg, praesidentin@uni-hamburg.de, AIAA fellow.
§ University of British Columbia, pfrommer@phas.ubc.ca .

electron density is one of the key parameter in the discharge, measurements of the cut-off density using a diagnostic microwave (8GHz to 12GHz) were used to validate and confirm the Langmuir probe data. Fabry-Perot interferometry measurements were carried out to determine the Doppler temperature of the plasma yielding values between 2000 K and 3000 K. For this purpose, the hyperfine structure of the emission lines under investigation had to be resolved and simulated. The results of the hyperfine structure splitting are in good agreement with experiments on an SPT thruster in France [7]. In addition, a Corona-type equilibrium was modeled, using results from the described measurements and excellent consistence could be derived by comparison with emission spectra [8]. Although the microwave plasma is substantially different from the ion thruster plume, particularly in terms of pressure, the properties of the charged particles determined in this investigation are in the same regime as those reported for the plasma state in the discharge chamber of ion thrusters [9], [10]. Therefore, the results from the microwave-generated plasma indicate a successful application to the ion thruster plasma inside the discharge chamber.

Recently, the LIF measurements on the cold gas cell have been conducted with a refined set up including a pump laser being changed from an Excimer laser to a NdYAG laser which provides a smaller pulse duration at almost the same pulse energy. Although the performance of the system could be remarkably increased in terms of signal to noise ratio, the required pressures for an investigation of the ion thruster plume could not be reached yet.

Emission spectroscopic measurements have been performed yielding axial and radial profiles of excitation temperatures and particle densities under the assumption of Boltzmann distributions. Although a set up for Fabry Perot measurements is completed, no data have been taken yet, therefore a more detailed excitation model such as the Corona model could not yet be applied.

II. Two-photon laser-induced fluorescence on neutral xenon in a cold gas cell

The LIF results in a cold gas cell with the Excimer laser have already been reported in [4] and [17]. Recently, the pumping laser has been replaced by a NdYAG laser which provides a smaller pulse duration at almost the same pulse energy yielding remarkable improvements in signal to noise ratio of the fluorescence signal. The minimum pressure for fluorescence detection is presently $5.7\ 10^{-3}$ hPa. Unfortunately, this value is still by two orders of magnitude higher than the pressure in the plume of the ion thruster.

In addition to the conventionally used excitation scheme [12, 4], different possibilities for the excitation of neutral Xeneon have been initially investigated (Eichhorn AIAA). First experiments indicate that they might show higher fluorescence signals therefore reducing the minimal achievable pressure at lower background signal due to spontaneous plasma emission.

The excitation of ionized Xenon using three photon transitions as required due to the high excitation energies and already proposed in literature [12] has been investigated theoretically [18]. Unfortunately, the application to the ion thruster plume as well as to the discharge chamber seems to be unrealistic with the presently available set up. A more detailed discussion is given in [19].

III. Experimental set up for thruster operation and optical diagnostics

The ion thruster is operated in a vacuum chamber with a diameter of 2 m and a length of 4 m, equipped with an oil diffusion pump system to achieve sufficient vacuum quality for ion thruster operation. The system consists of two oil diffusion pumps with a pumping speed of 50000 l/min. Background pressures of less than 10^{-6} hPa without gas flow and $3\ 10^{-5}$ mbar in operation with a mass flow of 4 SCCM xenon were achieved. The thruster is operated in grounded mode, only for start up, a glowing wire is used for electron generation. The most stable start up configuration has been achieved with tungsten wires mounted at a distance of 58 mm to the acceleration grid. Unfortunately, the mounting of these wires limits the optical access to the region close to the grid. Figure 11 shows a picture of the RIT-10 in operation. Although the wires are inactive they slightly glow due to interaction with the ion beam.

For the emission spectroscopic measurements, the optical set up was placed on top of the vacuum chamber as shown in figure 1. Focussing optics with one flat and one spherical mirror were used to image one axial region between 60 mm and 160 mm distance to the acceleration grid of the thruster simultaneously on the CCD chip. Shorter distances to the grid were not possible due to the mounting of the glowing wires which were used for igniting the thruster. During operation these wires were shut down and the thruster was operated in grounded mode. However, the interaction between the wires and the ion beam caused a disturbed region limiting the useable range of the detected area to a minimum distance of about 75 mm to the grid. Radial scans between the middle axis and an outer radial position of 45 mm were preformed by moving the whole set up across the optical window with a step size of 10 mm. A spectrometer with a focal length of 300 mm, a grating with 300 grids/mm and an open electrode

CCD camera with 1024 pixels x 256 pixels were used. A wavelength range between 360 nm and 1035 nm was covered by three individual measurements at each measurement position. Two thruster conditions with a xenon flow of 4 SCCM and 8 SCCM were investigated. Figure 2 shows a sketch of the set up and Table 1 resumes the characteristic properties of the thruster and the optical set up.

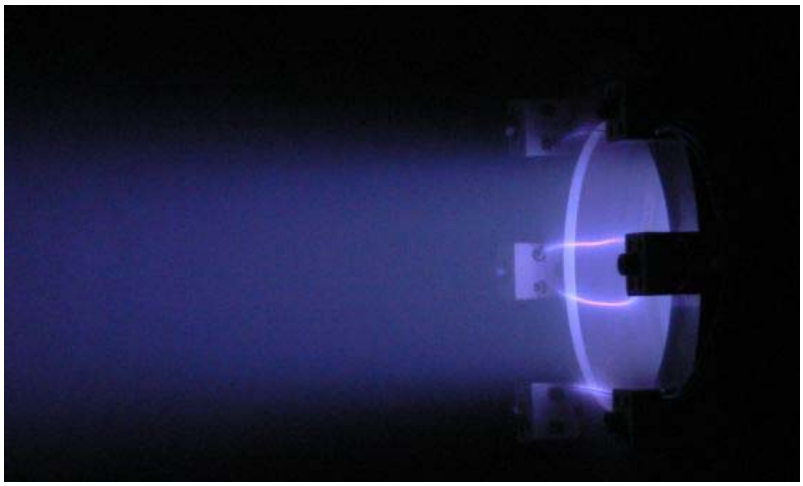

Figure 1. RIT-10 in operation.

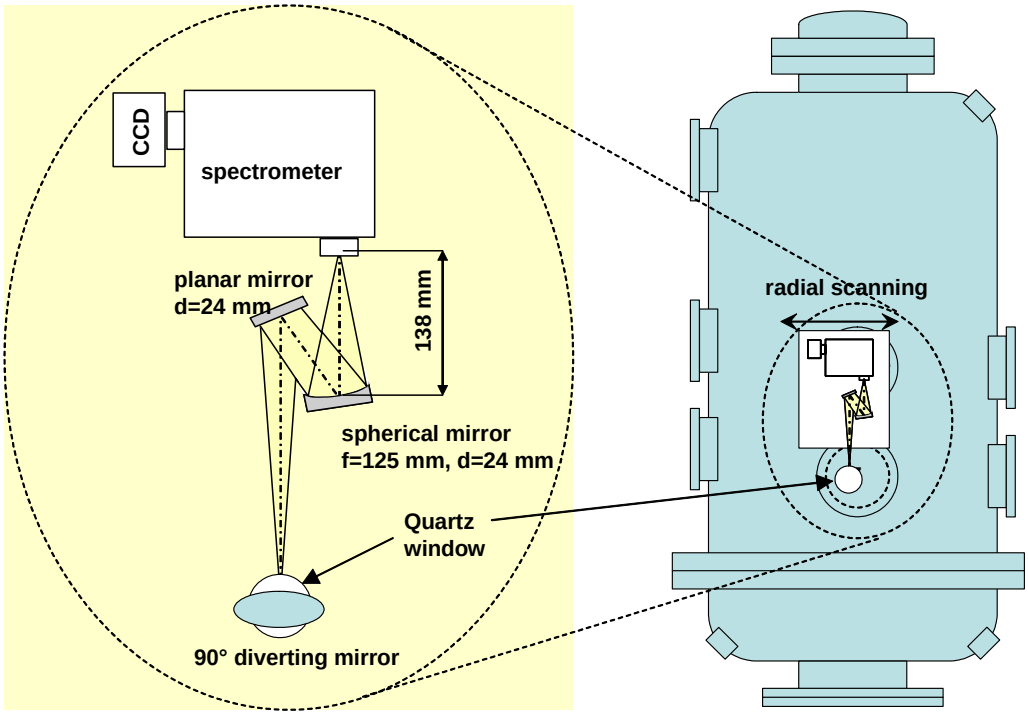

Figure 2. Emission spectroscopic set up .

Spectrometer	Acton 300i	
CCD-camera	Andor DU920N-OE, 1024 pixels x256 pixels, open electrode	
Grating	300 grinds/mm	
Wavelengtzh ranges	360nm-640nm / 562nm-838nm / 764nm-1034nm	
Edge filters (supression of 2. order)	GG375 / OG550 / OG550	
Pixel resolution	between 0.262 nm and 0.276 nm	
Spatial resolution	radial 0:4 mm, axial 3.9 mm	
Thruster	RIT-10	
Volume flow Xenon /SCCM	4	8
RFG power /W	90	60
Voltages (PHV/NHV) /V	900/-200	900/-200
Currents (PHV/NHV) /mA	153/-1.3	162/-4.25
Background pressure before test /mPa	0,134	0.21
Presure with RIT-10 in operation /mPa	1,94	4,81

Table 1. Characteristic data of thruster and optical set up.

For the Fabry Perot set up (FPI), the light is collected with a Quartz lens and focussed on an optical fibre. The fibre is connected to a fed a Burleigh interferometer. The light is expanded through another lens system to a collimated beam with a diameter of 22 mm and after passing the semi-permeable coplanar mirrors (reflectivity 94 %) of the FPI cavity, it is focussed (f=200 mm) to an aperture with a diameter of d=0.2 mm which replaces the entrance slit of the following spectrometer (Acton 300i; grating 600 lines mm) which acts as a spectral filter. At its exit slit a photomultiplier (Hamamatsu R928) detects the light, spectrally resolved by the FPI. The small focal length of the focussing lens of 150 mm yields in combination with the fibre diameter of 0.7 mm a rather poor spatial resolution in the plume with a diameter of the measured spot of about 30 mm. Radial and axial scans are performed by moving the focussing lens across the detection window. However, the large measured area causes overlapping of the single measured positions. The set up is completed but unfortunately, no data could be taken yet.

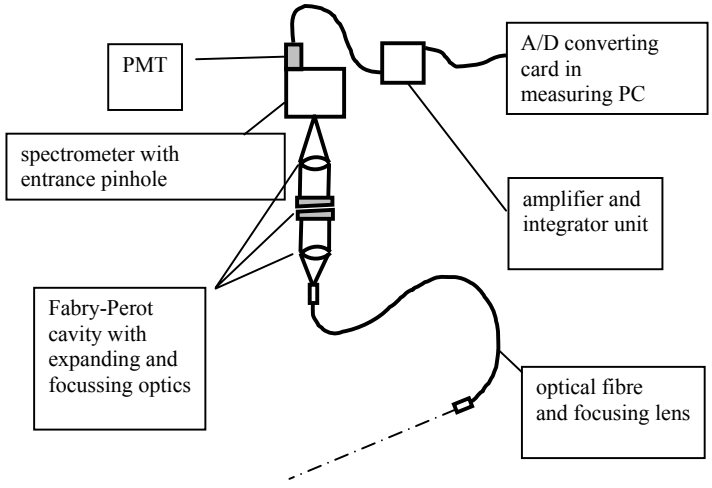

Figure 3. Optical set-up for Fabry-Perot interferometry.

IV. Results of emission spectroscopic measurements in the ion thruster plume

The emission spectroscopic measurements were calibrated using a Ulbricht sphere which was calibrated to spectral radiance. For the calibration, the lamp was placed inside the (not evacuated) tank and moved to the different measurement positions thus covering all influences on the measurement. Changes due to the missing vacuum during calibration are not expected since air is optically thin in the wavelength region of interest. The weak emission of the plume required acquisition times of 50 s for each measurement. Since the emission of the calibration lamp was much stronger it required remarkably shorter acquisition times. The ratio of the acquisition times was used for scaling down the signals, the linearity of the detector was checked in a separate measurement. Since a Corona model which was successfully used in the preparatory measurements with a microwave generator[8, 17] requires additional parameters such as electron density and temperature and gas temperature which are not available yet, the evaluation is restricted to the assumption of a Boltzmann distribution of the electronically excited states. Figure 4 shows a measured spectrum on the thruster axis at a distance of 101 mm to the acceleration grid at the 8 SCCM condition. The XeI and XeII lines used for further investigation are marked by arrows.

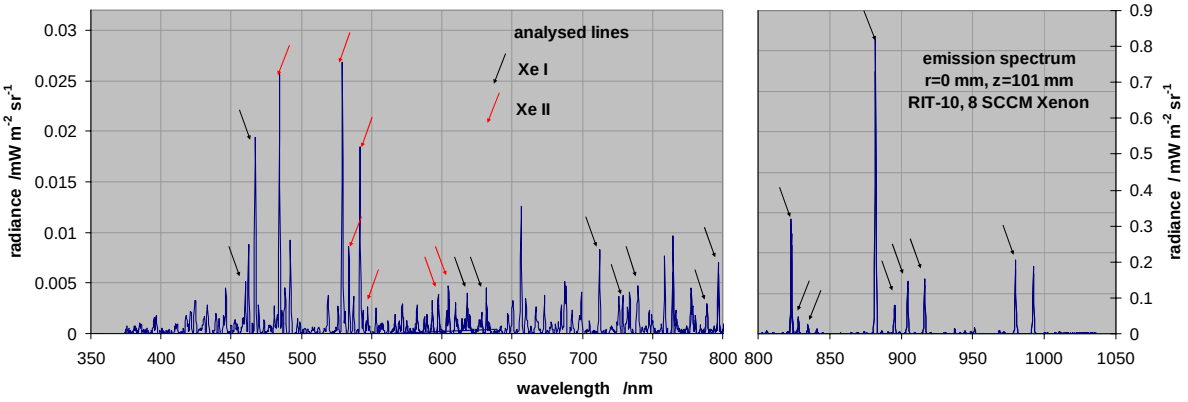

Figure 4. Emission spectrum on the thruster axis at a distance of 101 mm to the acceleration grid. XeI and XeII lines used for further analysis are marked by arrows.

The transition probabilities used for the analysis of the spectra were taken from literature. Since strongly diverging values were found for Xe I, averaged transitions probabilities were used which emanated from the preliminary investigations of the microwave plasma [8, 17]. For Xe II, the most recent data from DiRocco[29] was used. However, other literature data is presented as well. Tables 2 and 3 show a comparison of the different literature data and the values used for the present interpretation.

With these transition moments, an electronic excitation temperature can be determined if a distribution function can be assumed. An equilibrium assumption would yield a Boltzmann distribution to be used which relates the different electronically excited states one to another with a temperature which is ruling the distribution function:

$$\frac{n_{r,l}}{n_{r,m}} = \frac{g_{r,l}}{g_{r,m}} \, \mathrm{e}^{-\frac{E_{r,l}-E_{r,m}}{k_B T}}$$

By taking the logarithm this equation can be rewritten in the form of a straight line equation if the logarithmic terms are plotted versus the excitation energies for different emission lines with e being the intensity of each individual line and -1/Texc the slope of the straight line.

$$-\frac{E_k}{k_B T_{exc}} = \ln\left(\frac{\lambda \cdot \varepsilon}{g_k A_{ki}}\right) - \ln\left(\frac{n_r \cdot hc}{4\pi Z_r}\right)$$

The second term on the right hand side can be neglected if only one ionization stage is present since it only yields an offset in the obtained straight line and does not influence the excitation temperature. If emission lines of different ionization stages are to be evaluated together, the ratio of the corresponding particle densities and of the partition functions has to be taken in account in addition. To perform the Boltzmann plot rather than determining the excitation temperature only from the ratio of two lines gives the advantage of being able to judge the initial assumption of a Boltzmann distribution from the agreement of the measured data with the resulting straight line. Under and over populations of different levels can be extracted from this plot.

wavelength	transition	g_k	Einstein transition moment of XeI A_{ik} $[10^6 \frac{1}{s}]$							
$[nm]$	i - k		a)	b)	c)	d)	e)	f)	g)	used
450,1	6s$\left[\frac{3}{2}\right]$-6p'$\left[\frac{1}{2}\right]$	3	0,97	1,46		1,9				1,44
452,47	6s$\left[\frac{3}{2}\right]$-6p'$\left[\frac{3}{2}\right]$	5	0,27	0,46	0,4	0,25				0,35
458,27	6s$\left[\frac{3}{2}\right]$-6p'$\left[\frac{1}{2}\right]$	1	1,5			0,33	3,02		0,39	1,31
462,43	6s$\left[\frac{3}{2}\right]$-7p$\left[\frac{3}{2}\right]$	5	0,31	2,18		2,2			0,42	1,28
467,1	6s$\left[\frac{3}{2}\right]$-7p$\left[\frac{5}{2}\right]$	7	3,2	2,84		2,9	3,69			3,16
473,42	6s$\left[\frac{3}{2}\right]$-6p'$(\left[\frac{3}{2}\right]$	5	0,77			1,5	1,07			1,11
480,7	6s$\left[\frac{3}{2}\right]$-7p$\left[\frac{1}{2}\right]$	1	2,2		5	2,6	5,12		1,52	3,29
482,97	6s$\left[\frac{3}{2}\right]$-7p$\left[\frac{3}{2}\right]$	3	0,47			2,1	1,29			1,29
581,45	6p$\left[\frac{5}{2}\right]$-9d$\left[\frac{5}{2}\right]$	5						0,93		0,93
619,83	6p$\left[\frac{1}{2}\right]$-9s$\left[\frac{3}{2}\right]$	5							0,66	0,66
631,81	6p$\left[\frac{5}{2}\right]$-8d$\left[\frac{7}{2}\right]$	9							2,7	2,7
684,66	6p$\left[\frac{5}{2}\right]$-7d$\left[\frac{3}{2}\right]$	5					2,6			2,6
688,22	6p$\left[\frac{5}{2}\right]$-7d$\left[\frac{7}{2}\right]$	7						5,83	6,4	6,12
711,96	6p$\left[\frac{5}{2}\right]$-7d$\left[\frac{7}{2}\right]$	9							8,39	8,39
728,53	6p$\left[\frac{3}{2}\right]$-7d$\left[\frac{5}{2}\right]$	5							4,09	4,09
739,38	6p$\left[\frac{3}{2}\right]$-7d$\left[\frac{5}{2}\right]$	7							4,89	4,89
788,74	6s'$\left[\frac{1}{2}\right]$-6p'$\left[\frac{1}{2}\right]$	1	20,7			42	21,8		10,4	23,73
796,73	6s'$\left[\frac{1}{2}\right]$-7p$\left[\frac{3}{2}\right]$	3	2,51				5,91			4,21
823,16	6s$\left[\frac{3}{2}\right]$-6p$\left[\frac{3}{2}\right]$	5	18,6	28,6	29	23	24,9			24,82
828,01	6s$\left[\frac{3}{2}\right]$-6p$\left[\frac{1}{2}\right]$	1	33,3	34	33	36	44,5			36,95
834,68	6s'$\left[\frac{1}{2}\right]$-6p'$\left[\frac{3}{2}\right]$	5	20,9		29	35	26,4			27,83
840,92	6s$\left[\frac{3}{2}\right]$-6p$\left[\frac{3}{2}\right]$	3	2,5	3,1		2,1	1,84			2,39
881,94	6s$\left[\frac{3}{2}\right]$-6p$\left[\frac{5}{2}\right]$	7	29,4	30		30	39,2			32,15
895,22	6s$\left[\frac{3}{2}\right]$-6p$\left[\frac{3}{2}\right]$	5	7,9	7,5	8	11	10,5			8,98
904,5	6s$\left[\frac{3}{2}\right]$-6p$\left[\frac{5}{2}\right]$	5	9,1	12,4	13,8	10	10,7			11,2
916,26	6s$\left[\frac{3}{2}\right]$-6p$\left[\frac{3}{2}\right]$	3	27,7	21,7		25	31,6			26,5
980	6s$\left[\frac{3}{2}\right]$-6p$\left[\frac{1}{2}\right]$	3	24,8	31,1	26,6	21	31			26,9

Table 2: *Transitin moments of Xe II, published in literature (a)=Horiguchi et al. (1981)[20], b)=Sabbagh & Sadeghi (1977) [21], c)=Karimov & Klimkin (1971) [11], d)=Chen & Garstang (1970) [22], e)=Aymar & Coulombe (1978) [23], f)=Martin et al. (1985) [24], g)=Miller & Roig (1973) [25]) and values used fort he present investigation*

wavelength	transition	g_k	Einstein coefficient of XeII A_{ik} $[10^6 \frac{1}{s}]$				
$[nm]$	i - k	h)	i)	j)	k)	l)	m)
484,43	6s(4)P$\left[\frac{5}{2}\right]$ -6p(4)D$\left[\frac{7}{2}\right]$	8	147,5	86,8	77	124,5	93,4
529,22	6s(4)P$\left[\frac{5}{2}\right]$ -6p(4)P$\left[\frac{5}{2}\right]$	6	109,5	90,4	232	114,3	66,3
533,94	6s(4)P$\left[\frac{5}{2}\right]$-6p(4)P$\left[\frac{3}{2}\right]$	4	86,8	66,9	188	70,3	45,83
541,92	6s(4)P$\left[\frac{5}{2}\right]$ -6p(4)D$\left[\frac{5}{2}\right]$	6	101,8	64,9	213	90,7	53,28
547,26	5d(4)D$\left[\frac{5}{2}\right]$ -6p(4)D$\left[\frac{7}{2}\right]$	8			49		
597,65	6s(4)P$\left[\frac{5}{2}\right]$ -6p(4)P$\left[\frac{3}{2}\right]$	4	15		109		4,96
605,12	5d(4)D$\left[\frac{5}{2}\right]$ -6p(4)P$\left[\frac{5}{2}\right]$	6	20,5	52		21,3	21

Table 3: *Transition moments of Xe II, published in literature (h)=Garpman & Spector (1976)[26], i)=Gigosos et al. (1994) [27], j)=Manzella (1993) [28], k)=DiRocco et al. (2000) [29], m)=Sherbini (1976) [30]).*

To apply this method to measured spectra, the spectrally integrated intensity of each emission line (in the following called line intensity) has to be determined. Therefore, the spectrum has to be integrated over the line width

for the lines of particular interest. To account for continuum radiation, uncertainties in background correction and stray light it is subtract a triangle given by the pixels next to the edges of the line. Due to the large amount of data, this was done automatically. Some uncertainty results from this procedure if the emission lines are very weak. The process of manually controlling the evaluation is still ongoing, therefore the results are regarded as preliminary for the time being. Figure 5 shows examples for the Boltzmann plots of measured spectra taken on the middle axis at a distance of 101 mm to the acceleration grid for the two thruster conditions.

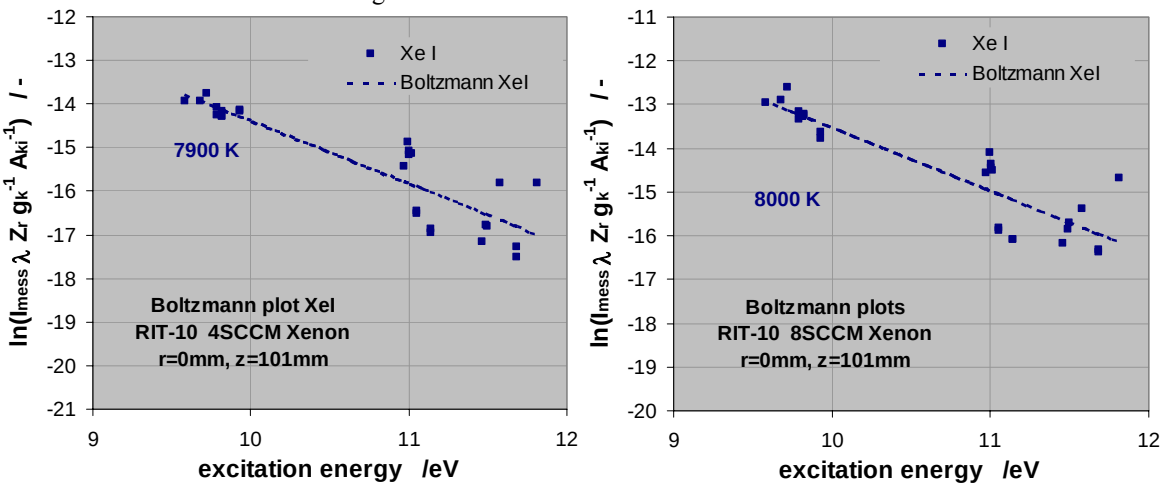

Figure 5. Boltzmann plots for the selected XeI and XeII lines at the two thruster conditions at the middle axis in a distance of 101 mm to the acceleration grid.

The Boltzmann plots show that the population densities do not completely agree with a Boltzmann distribution. In the case of 4 SCCM xenon, the scattering of the different values around the straight line is in general slightly higher than at 8 SCCM. A separate temperature determination from the XeII lines is not possible since the energy levels are too close together. Therefore the evaluation will be restricted to the XeI lines. A combined excitation temperature can not determined straight forward since the ratio of the particle densities which is still unknown would be needed for the Boltzmann distribution. The radial and axial profiles of the resulting excitation temperatures based on the emission of neutral xenon are given in figures 6 and 7.

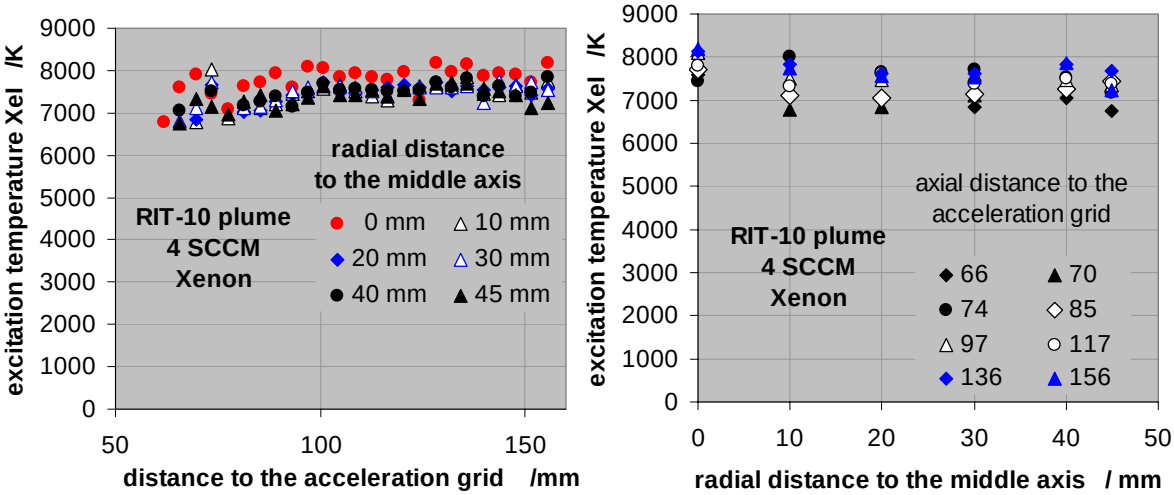

Figure 6. Radial and axial profiles of excitation temperature of neutral xenon for the 4 SCCM condition.

In general, a flat radial profile can be seen at all axial positions. The temperature rises up to a distance of about 100 mm to the acceleration grid and stays almost constant from there to higher distances. The inconsistency at 70 mm to the grid is caused by the tungsten wire which is used as neutralizer during ignition. At both conditions the temperatures are in the order of 8000 K, slightly higher with 8 SCCM than with 4 SCCM.

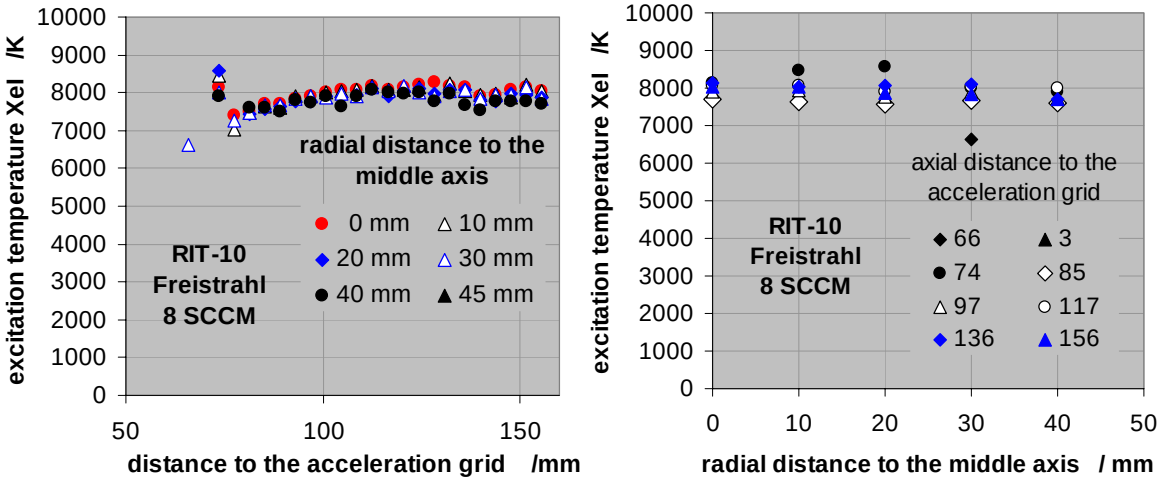

Figure 7. Radial and axial profiles of excitation temperature of neutral xenon for the 8 SCCM condition.

To get an idea of the meaning of the obtained temperatures, the Boltzmann distribution was extrapolated to the ground state to give an estimate of neutral and ion particle densities. The particle densities of the electronically exited states can be computed by

$$\varepsilon_{r,k,i} = \frac{h\nu_{r,k,i}}{4\pi} A_{r,k,i} n_{r,k,i} \quad .$$

The Boltzmann distribution also relates the total particle density to the electronically excited ones by

$$n_{r,k} = \frac{g_{r,k}}{U(T_{anr,r})} n_r \exp\left(-\frac{E_{anr,r,k}}{kT_{anr,r}}\right)$$

For the temperature range of concern, the partition function is only a weak function of temperature and clearly dominated by the low energetic states (i.e. the ground state). From the Boltzmann plots it seems that the 8 SCCM condition is slightly closer to equilibrium than the 4 SCCM one. Therefore this estimation was performed for the 8 SCCM condition. Figure 8 shows the neutral and ion particle densities calculated with the excitation temperature determined from neutral xenon. For each line, the complete particle density was computed separately. The plotted curves represent the average value of all lines, the error bars give the corresponding maximum and minimum values.

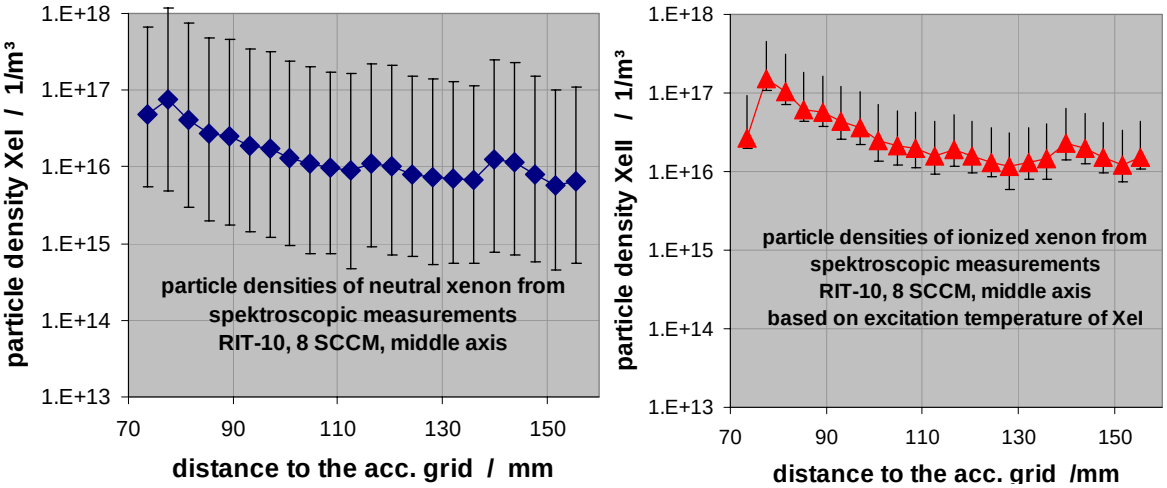

Figure 8. Boltzmann plots for the selected XeI and XeII lines at the two thruster conditions at the middle axis in a distance of 101 mm to the acceleration grid.

Both particle densities are in the same order of magnitude, the ion density slightly higher than the neutral one, and decrease by one order of magnitude from the upstream to the downstream border of the observed region.

To get an idea about the meaning of these particle densities, a rough estimation based on the thermal state equation and on the thruster performance data can be made. Based on the measured pressure of 4.8 mPa

$$p = nkT$$

yields particle densities of 4 10^{17} m^{-3} to 4 10^{16} m^{-3} for temperatures between 1000K and 10000K, respectively. This is in surprisingly good agreement with the density values obtained from the spectroscopic measurements. At the same time, this would indicate that the electronic excitation would be in equilibrium with the translational temperature. This may indicate that either equilibrium is reached which is somehow unlikely in the pressure range of concern or that the electronic excitation happens rather due to heavy particle collisions than to electronic excitation. This will be verified as soon as translational temperatures from the FPI and electron temperatures and densities from Langmuir probe measurements are available .

The ion density at the thruster exit can be estimated from the measured current to the extraction grid. For this estimation, a beam diameter of 120 mm and an ion velocity of 30 km/s were assumed yielding an ion density of 3 10^{15} m^{-3}. This is by two orders of magnitude lower than the values shown in figure 8. Although portions of the neutral gas due to the background pressure will probably be ionized by collisions with fast ions the question remains if this might increase ion density in such large amount. This question can probably be answered by measurements of electron density with Langmuir probes. As another possibility, the excitation of the ions might be caused by electrons provided by the above mentioned ionization process and obey a different excitation process. However, the ion densities shown in figure 8 are considered to be highly questionable until not verified by other measurements.

V. Fabry Perot interferomtry

The Fabry Perot interferometer acts as a high-resolution monochromator. From the Doppler broadening, the heavy particle temperature is to be determined. For xenon, the isotope shift due to the different masses of the nine stable isotopes and the hyperfine structure due to non-zero nuclear spins of two isotopes (^{129}Xe and ^{131}Xe) have to be taken into account yielding a total of 21 single lines for one electronic transition. Both effects are of the same order and have therefore to be considered. The magnetic field in the plasma and hence the Zeeman effect can be neglected. The isotope shift has been treated comprehensively in literature, and data for the field shift (FS) and the normal (NMS) and specific mass shift (SMS) have been taken from [13]. The frequency shift of a transition *i* between two isotopes with the masses A, A0, respectively, can be calculated as:

$$\delta\nu_i^{AA'} = \delta\nu_{i,FS}^{AA'} + \delta\nu_{i,NMS}^{AA'} + \delta\nu_{i,SMS}^{AA'}$$

Because the nuclear spin of ^{131}Xe (I=3/2) is > 1, not only the electrical dipole interaction as for ^{129}Xe (I=1/2) has to be considered but also the electrical quadrupole interaction. The hyperfine (HF) effect does not split the energy levels of the fine structure into more sublevels but shifts them towards different energies. In the absence of a magnetic field, each HF-level is 2F +1-times degenerated, if F is the quantum number for the total angular momentum (F=J+I). The energy of the hyperfine structure levels is calculated using

$$E_{HFS} = E_{Dip}(I,J,F) + E_{Quad}(I,J,F) = \frac{C}{2}\cdot A + \frac{B}{4}\cdot\frac{\frac{3}{2}C(C+1) - 2I(I+1)J(J+1)}{I(2I-1)J(2J-1)}$$

C is hereby a shortcut for C = F(F + 1) − J(J +1) − I(I + 1). A and B are the hyperfine constants and have been taken from [14]. For a complete simulation the line strengths have to be determined as well. They obey their statistical weights and can be calculated as written in [15]. Table 4 shows the isotope shifts, their natural abundances and the necessary data for the hyperfine structure calculation of ^{131}Xe and ^{129}Xe.

A $[amu]$	$\delta\nu_{S232}^{A,136}$ $[MHz]$	natural abundance [%]
124	419	0.0096
126	335	0.009
128	263	1.92
129	271	26.44
130	203	4.08
131	229	21.18
132	149	26.89
134	97	10.44
136	0	8.87

^{131}**Xe** ; $I = \frac{3}{2}$; $J' = J'' = 2$

F'	F''	C'	C''	line strength S	ΔE $[MHz]$
3.5	3.5	6	6	0.343	-1380.87
3.5	2.5	6	-1	0.057	1312.70
2.5	3.5	-1	6	0.057	-2333.61
2.5	2.5	-1	-1	0.173	359.96
2.5	1.5	-1	-6	0.07	1968.29
1.5	2.5	-6	-1	0.07	-283.10
1.5	1.5	-6	-6	0.08	1325.23
1.5	0.5	-6	-9	0.05	2163.97
0.5	1.5	-9	-6	0.05	954.39
0.5	0.5	-9	-9	0.05	1793.13

^{129}**Xe** ; $I = \frac{1}{2}$; $J' = J'' = 2$

F'	F''	C'	C''	line strength S	ΔE $[MHz]$
2.5	2.5	2	2	0.56	1492.37
2.5	1.5	2	-3	0.04	-4469.76
1.5	2.5	-3	2	0.04	3723.57
1.5	1.5	-3	-3	0.36	-2238.55

Table 4. Natural abundance of xenon isotopes, isotope shifts and the necessary data for the hyperfine structure calculation of ^{131}Xe and ^{129}Xe.

After determining the different intensities, the lines are broadened with a Lorentzian profile for the apparatus broadening (0.6 pm in the experiments with the microwave generator) and a Gaussian profile for the Doppler broadening. The best fit between measured and simulated profile yields the heavy particle temperature. Figure 9 shows a comparison between data measured at the mircrowave plasma and theoretically calculated line profile for the observed transition of neutral xenon at a wavelength of 823.16 nm. 21 components of this spectrum are indicated with Dirac delta peaks, 3 times enlarged. Measurements in the RIT-10 plume are being prepared but no data is available yet.

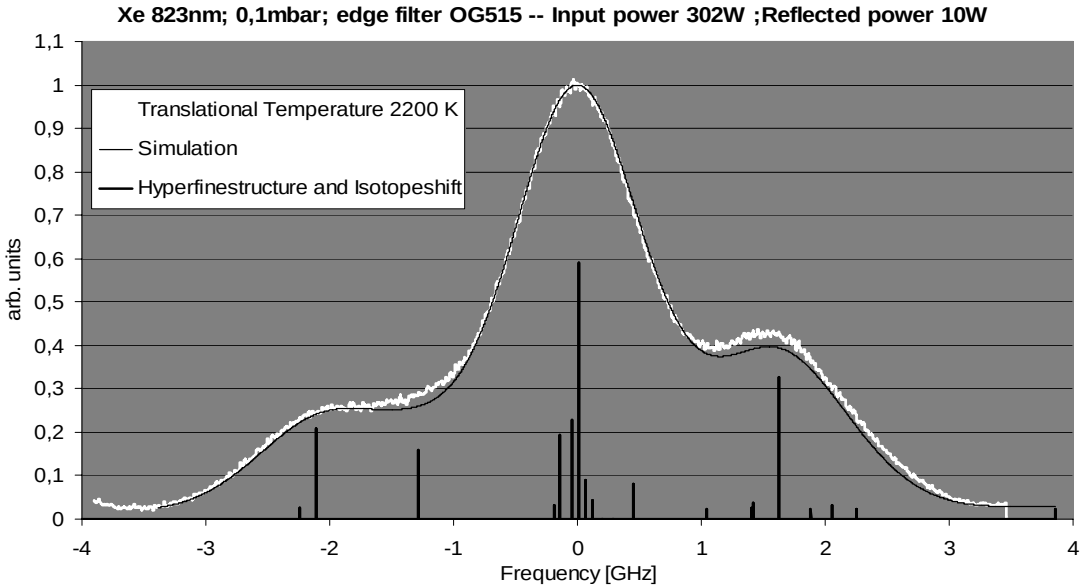

Figure 9. Measured and calculated hyperfine structure of the 823.16 nm transition of neutral xenon.

VI. Conclusion and further plans

Emission spectroscopic measurements in the plume of a RIT-10 ion thruster have been performed at two thruster conditions. From these measurements, excitation temperatures in the order of 8000K could be obtained under the assumption of Botzmann distributions for the electronically excited levels of neutral xenon. At one position particle densities of neutral and ionized xenon were computed, again under equilibrium assumptions. The neutral densities obtained are in surprisingly good agreement with gas dynamic estimations based on the measured background pressure. The ion densities are comparatively high and lack for a verification by other measurement methode such as Langmuir probe measurements. A Fabry-Perot interferometry set up has been installed for the determination of heavy particle temperature from the Doppler broadening but no data is available yet. Measurements with two photon laser induced fluorescence on a cold gas cell have shown that the pressure in the RIT-10 plume is most probably too low for reliable measurements of particle densities with the existing set up. However, new excitation schemes are

under investigation to possibly overcome these restrictions. A more promising application would be measurements inside the discharge chamber where pressures are remarkably higher. For this purpose, optical access to the discharge chamber would be necessary possibly by the use of glas discharge chambers as used in former RIT designs.

Acknowledgments

This work was supported by the Deutsches Zentrum für Luft- und Raumfahrt (DLR). The authors wish to thank Evangelisches Studienwerk Villigst e.V. for financial and idealistic support through a Ph.D. scholarship for Christoph Eichhorn. Furthermore, all colleagues and students who helped in building up the vacuum facility and the experiments. Finally, the authors wish to thank EADS-ST for providing the ion thruster and for support with the installation and operation at IRS.

References

[1] Auweter-Kurtz, M., Feigl, M., Winter, M.: Diagnostic Tools for Plasma Wind Tunnels and Reentry Vehicles at the IRS, RTO-EN-8. AC/323(AVT)TP/23, RTO Educational Notes 8, April 2000; von Karman Institute for Fluid Dynamics, RTO AVT/VKI Special Course on Measurement Techniques for High Enthalpy Plasma Flows, Belgium, Oktober 1999.

[2] M. Auweter-Kurtz, N. Semenova, M. Winter, S. Löhle: Plasmadiagnostik an Ionentriebwerken, Technischer Statusbericht für die Zeit vom 1.2.2002 bis zum 1.7.2003, Stuttgart, 2003.

[3] Basner, H., Killinger, R., Leiter, H., Müller, J.: Advantages and Applications of the RF-Ion Thruster RIT, AIAA 2001-3494, 2001.

[4] N. Semenova, M. Auweter-Kurtz and , M. Winter, „Development of Laser-Spectroscopic Techniques on Xenon for RIT-Ion Thruster Plume Investigations", AIAA-2004-3962, 40th AIAA/ASME/SAE/ASEE Joint Propulsion Conference and Exhibit, 11-14 July 2004, Fort Lauderdale, FL, USA.

[5] Pfrommer, T., Auweter-Kurtz, M., Holzhauer, E., Semenova, N., and Winter, M., "Emission Spectroscopy and Double Langmuir Probe Measurements on Xenon for future Application with Radio-Frequency Ion Thrusters (RIT)," ,IAC-04-S.P.02, 55th International Astronautical Congress, Vancouver, BC, Canada, October, 4 – 8 ,2004..

[6] Thomas Pfrommer, Monika Auweter-Kurtz and Michael W. Winter, Fabry-Perot Interferometry on Xenon for Future Application with Radio-frequency Ion Thrusters (RIT), Space Technology Education Conference STEC 2005, Aalborg, Denmark, April 2005.

[7] Mazouffre, S., Pagnon, D., Lasgorceix, P., and Touzeau, M., "Temperature of Xenon atoms in a stationary plasma thruster," 2003, presented at the IEPC 2003.

[8] Pfrommer, T.: Charakterisierung eines Niederdruck-Xenon-Plasmas über emissionsspektroskopsiche Messungen, IRS-05-024, Diploma thesis, Institute of Space Systems, University of Stuttgart, Stuttgart, Germany, 2005

[9] Homepage of the University of Gießen, Germany:
http://nathanderweise.physik.uni-giessen.de/~dhasselk/Diverses/Physik_alles.html

[10] Daniel A. Herman and Alec D. Gallimore, Discharge Chamber Plasma Structure of a 30-cm NSTAR-type Ion Engine, AIAA-2004-3794.

[11] Karimov R.G. and Klimkin V.M.: XeI and XeII radiative lifetime and transition probabilities, Sov. Phys. J., Vol. 14, p.307, 1971.

[12] CROFTON, MARK: Measurement of neutral Xenon density profile in an ion thrusters plume, AIAA-96-5151, 32 nd Joint Propulsion Conference, Lake Buena Visat, FL, USA, July, 1 – 3, 1996.

[13] Behringer,K., Fantz, U.: Spectroscopic Diagnostics of Glow Discharge Plasmas with Non-Maxwellian Electron Energy Distributions, J. Phys. D: Appl. Phys. 27

[14] Schaefer, H.: Isotopieverschiebug im XenonI-Spektrum und Kerndeformation der stabilen Xenon-Nuklide, Dissertation, PhilippsUniversiaet Marburg/Lahn, 1973

[15] Wiegand, B.: Untersuchungen der Hyperfeinstruktur optischer Übergänge in den Spektren von einfach geladenen Xenon- und Eisenionen, Dissertation, Philipps Universiaet Marburg/ Lahm, 2001

[16] Moore, C.: Atomic Energy Levels, Vol. III, National Bureau of Standards, Washington, 1958

[17] Michael W. Winter, Monika Auweter-Kurtz, Thomas Pfrommer and Nataliya Semenova: Plasma Diagnostics on Xenon for Application to Ion Thrusters, IEPC-2005-079, 29th International Electric Propulsion Conference, Princeton University, NJ, USA, 31. October - 4. November 2005.

[18] Christoph Eichhorn, Michael M. Winter, Monika Auweter-Kurtz, and Stefan Löhle: Theoretical and Experimental Approach of Multi-Photon Spectroscopy on Xenon for Application on Ion Thruster Plasma Parameter Investigations, AIAA_2007_3878, 38th AIAA Plasmadynamics and Lasers Conference, Miami, Florida, June 25-28, 2007.

[19] C. Eichhorn, M. Auweter-Kurtz, M. Winter: Multiphoton Spectroscopy on Xenon for application on ion thrusters plasma parameter investigations: Experiment and Theory, 30th International Electric Propulsion Conference, Florence, Italy, September 17-20, 2007

[20] Horiguchi, H., Chang, R., Setser, D.: 1981, Radiative Lifetimes and Two-body Collisional Deactivation Rate Coefficients in Ar for Xe(5p 56p), Xe(5p 56p') and Xe(5p57p) States, J.Chem.Phys 75, 1207
[21] Sabbagh, J., Sadeghi, N.: 1977, Experimental Transition Probabilities of some Xe I Lines, J.Quant. Spectrosc.Radiat. Transfer 17, 297
[22] Chen, C., Garstang, R.: 1970, Transitio Probabilities for Xenon I, J.Quant.Spec.Rad.Transfer 10, 1347
[23] M.Aymar and M.Coulombe: Theoretical transition probabilities and lifetimes in KrI and XeI spectra, Atomic Data and nuclear data tables, Vol. 21, 1978.
[24] Martin, P., Cabreros, J., Campos, J.: 1985, Transition Probabilities of 6p-nd (n=7,8,9) Lines of Xenon, Physical Review A 32, 3110
[25] Miller, M. H., Roig, R. H.: 1973, Transition Probabilities of Xe I and Xe II, Phys.Rev.A 8, 480
[26] Garpman, S., Spector, N.: 1976, Transition probabilities for the 5p(4)6p-5p(4)6s Array of XeII, J. opt.Soc. Am. 66
[27] Gigosos, M., Mar, S., Perez, C., de la Rosa, I.: 1994, Experimental Stark widths and shifts and transition probabilities of several XeII lines, Physical Review E 49
[28] Manzella, D. H.: 1993, Stationary Plasma Thruster Plume Emissions Presented as IEPC 93-097
[29] DiRocco, H., Iriarte, D., Pomarico, J.: 2000, Lifetimes and Trsansition Probabilities of Xenon II: Experiment Measurement and Theoretical Calculation, Eur.Phys.J. D 10, 19
[30] Sherbini, T.: 1976, Transition Probabilities and Raidative Lifetimes of singly ionized Xenon, J.Phys.B Atom.Molek.Phys. 9, 1665